Tribology Letters (2020) 68:106
https://doi.org/10.1007/s11249-020-01344-3

ORIGINAL PAPER

Surface Gel Layers Reduce Shear Stress and Damage of Corneal Epithelial Cells

Samuel M. Hart[1] · Eric O. McGhee[2] · Juan Manuel Urueña[1] · Padraic P. Levings[3] · Stephen S. Eikenberry[4] · Matthew A. Schaller[5] · Angela A. Pitenis[6] · W. Gregory Sawyer[1,2]

Received: 14 April 2020 / Accepted: 17 September 2020 / Published online: 6 October 2020
© Springer Science+Business Media, LLC, part of Springer Nature 2020

Abstract

Soft contact lenses are medical devices made from aqueous polymeric gels that are worn on the eye to correct refractive errors. These devices interrupt the natural contact pairing between the cornea and the eyelid and create two interfaces comprised of a synthetic material and the epithelia—contact lens surfaces versus (1) the cornea and (2) the eyelid conjunctiva. The cellular responses to friction and shear stress are thought to contribute to contact lens discomfort. This study performs direct contact shear experiments using in vitro biotribological experiments using a microtribometer equipped with a hydrogel membrane probe. Sections from commercial contact lenses are held in place on a spherically capped membrane probe during reciprocating sliding experiments against confluent monolayers of living human telomerase-immortalized corneal epithelial cells (hTCEpi). The contact lenses were loaded against the cell monolayers to physiological contact pressures between 400 and 1300 Pa under an applied load of 200 μN. The reciprocating distance was 3 mm, at a sliding speed of 1 mm/s, and the maximum duration of sliding was 1000 cycles. Five commercially available lenses (somofilcon A, stenfilcon A, etafilcon A, verofilcon A, and delefilcon A) were used to evaluate the cell layer responses to aqueous gels of differing composition, surface modulus, and lubricity. Cell damage was measured via propidium iodide staining and in situ fluorescence microscopy. The shear stresses varied from 16 ± 2 Pa (delefilcon A and verofilcon A) to 86 ± 12 Pa (stenfilcon A), and cell damage increased with increasing shear stress and increasing sliding duration. The two lens materials that have high water content surface gel layers (delefilcon A and verofilcon A) showed distinctly lower measures of cell damage as compared to the other lenses. Surface gel layers with a large polymer mesh size and high water content are shown to be an effective approach to lower the contact pressure, lower the friction coefficient, and thereby lower the shear stress and cell damage.

Keywords Contact lenses · Shear stress · Apoptosis · Fluorescence microscopy · Biotribometer

✉ W. Gregory Sawyer
wgsawyer@ufl.edu

1 Department of Mechanical and Aerospace Engineering, Herbert Wertheim College of Engineering, University of Florida, Gainesville, FL 32611, USA

2 Department of Materials Science and Engineering, Herbert Wertheim College of Engineering, University of Florida, Gainesville, FL 32611, USA

3 Department of Orthopaedics and Rehabilitation, College of Medicine, University of Florida, Gainesville, FL 32611, USA

4 Department of Astronomy, College of Liberal Arts and Sciences, University of Florida, Gainesville, FL 32611, USA

5 Division of Pulmonary, Critical Care and Sleep Medicine, College of Medicine, University of Florida, Gainesville, FL 32611, USA

6 Materials Department, College of Engineering, University of California, Santa Barbara, Santa Barbara, CA 93106, USA

1 Introduction

Among the softest creatures in the world are a diverse group of marine animals found in our oceans: anemones, hydroids and jellies. These fragile creatures are almost entirely made of water—they are aqueous gels, made from a crosslinked biopolymer (collagen) swollen in sea water to almost 95% [1, 2]. The eye's first line of defense against the external environment, the ocular tear film, is similar in water content; a thin stratified layer of moist epithelial cells protected by a mucinated aqueous gel (≈ 95% water), with the main difference being the labile and weak crosslinks of mucin [3]. The eye is a delicate, dynamic, and intricate biological system. The mucins present in the tear film (MUC1, MUC2, MUC4, MUC5AC, and MUC16) [4, 5] arrange into a graded gel layer [6–8] that serves to maintain hydration and clarity of the ocular surface, provide lubrication, and resist adhesion between the corneal and conjunctival epithelia during an eyeblink [9]. The volume of the tear film is estimated to be on the order of 8 ± 3 µL [8], and tear film thickness below 10 µm—estimates of the precorneal tear film based on reflectance spectra are on the order of 3 µm [10].

The diverse array of mucins in the ocular environment are broadly divided into two categories—membrane-attached mucins and secretory mucins. The membrane-bound mucins (e.g. MUC1) form the anchor layer for this gel network and the higher molecular weight secretory mucins (e.g. MUC5AC) develop into the lower density gel network. These mucins create a gel-spanning network through transient crosslinks (hydrogen and disulfide bonds) and even shorter-living physical entanglements [3]. The weak physical crosslinks and the large mesh size of mucin gels result in a surface with an intrinsically low shear stress during sliding, due to the large mesh size, high water content, and low yield stress. Once the shear stress exceeds a failure stress, the physical crosslinks break, shear thin [11], and then reform (heal) dynamically during the relaxation time between blinks. This fragile gel-spanning mucin network acts like a mechanical fuse limiting the stress that can be transmitted to the underlying epithelial cells. Ocular health and comfort are inexorably linked to the quality and stability of this functional fragile gel interface. This tear film contributes to homeostasis on the ocular surface, maintains clarity across the cornea, and provides a physical barrier against foreign debris [12] (e.g. pathogens, toxins, and particles) while permitting the rapid passage of selected gases, fluids, ions, and nutrients to the epithelial cells. Tear film stability, lubrication properties, and rates of evaporation are all determined by the integrated composition of the tear film: proteins, mucins, and lipids.

The eyes are almost continuously moving while awake, and frequently during sleep [13]. During a blink, the eyelid wiper accelerates to a maximum speed of approximately 100 mm/s, approaches the lower eyelid, and then retracts back; the entire process takes place in ≈ 100 ms [14]. Estimates of the maximum shear rate are on the order of 10^4–10^5 1/s depending on the assumptions regarding the thickness of the shearing zone [14] (Fig. 1a). Given the gradient in mucin composition and concentration across the tear film, the fluidized zone may be increasing in response to the sliding speed to maintain a nearly constant shear rate and shear stress during blinking and ocular movement. The contact pressure exerted on the cornea by the eyelid during this activity has not been directly measured, and undoubtedly depends on the degree to which the gel spreads contact across the contact zone—the contact pressure is estimated to be on the order of a few kPa.

Although rarely discussed as such, the contact lenses should be thought of as a foreign body in the ocular environment. The insertion of a soft contact lens into the ocular system clearly disrupts the natural system and creates two entirely new interfaces comprised of a synthetic material and the epithelia (contact lens versus conjunctiva and contact lens versus cornea) and fundamentally change the tissue/tissue contact mechanics. Traditionally, these hydrogels have high polymer content (≈ 50% water) in comparison to the ultra-high water content ocular gels (≈ 95% water). The physics of friction in aqueous gels and biological systems is widely studied with numerous experiments and models describing the mechanisms behind the lubrication of these materials [15–23] and the ubiquitous finding is that increased water content increases the lubricity.

Contact lens discomfort and dry eye discomfort may have a related underlying etiology where elevated levels of shear stress are responsible for initiating pain signaling through the release of proinflammatory cytokines [24, 25], which are recognized as important mediators of inflammatory pain [26] associated with the primary sensory neurons (nociceptors) that are abundant in the ocular tissues [27, 28]. The combination of increased contact pressure, disruption of the tear film, and the resulting frictional shear stress are thought to be key contributors to discomfort in contact lens wear [29]. A recent design strategy has been built around surface gel layers, which increase the water content and mesh size of the aqueous gel on the surface of the lenses [2, 21, 30, 31], Fig. 1b. In contrast to homogeneous lens materials, Fig. 1c, the lenses with surface gel layers aim to reduce the frictional shear stresses by dropping both the contact pressure and friction coefficient, Fig. 1d.

In hydrogels, as the water content increases, the mesh size (ξ) of the hydrogel network also increases [2, 21, 32]. The increase in mesh size causes a dramatic decrease in the elastic modulus ($E \propto \xi^{-3}$) [33, 34] of the gel and also causes a reduction in the friction coefficient ($\mu \propto \xi^{-1}$) [21]. Increasing mesh size thereby reduces the frictional

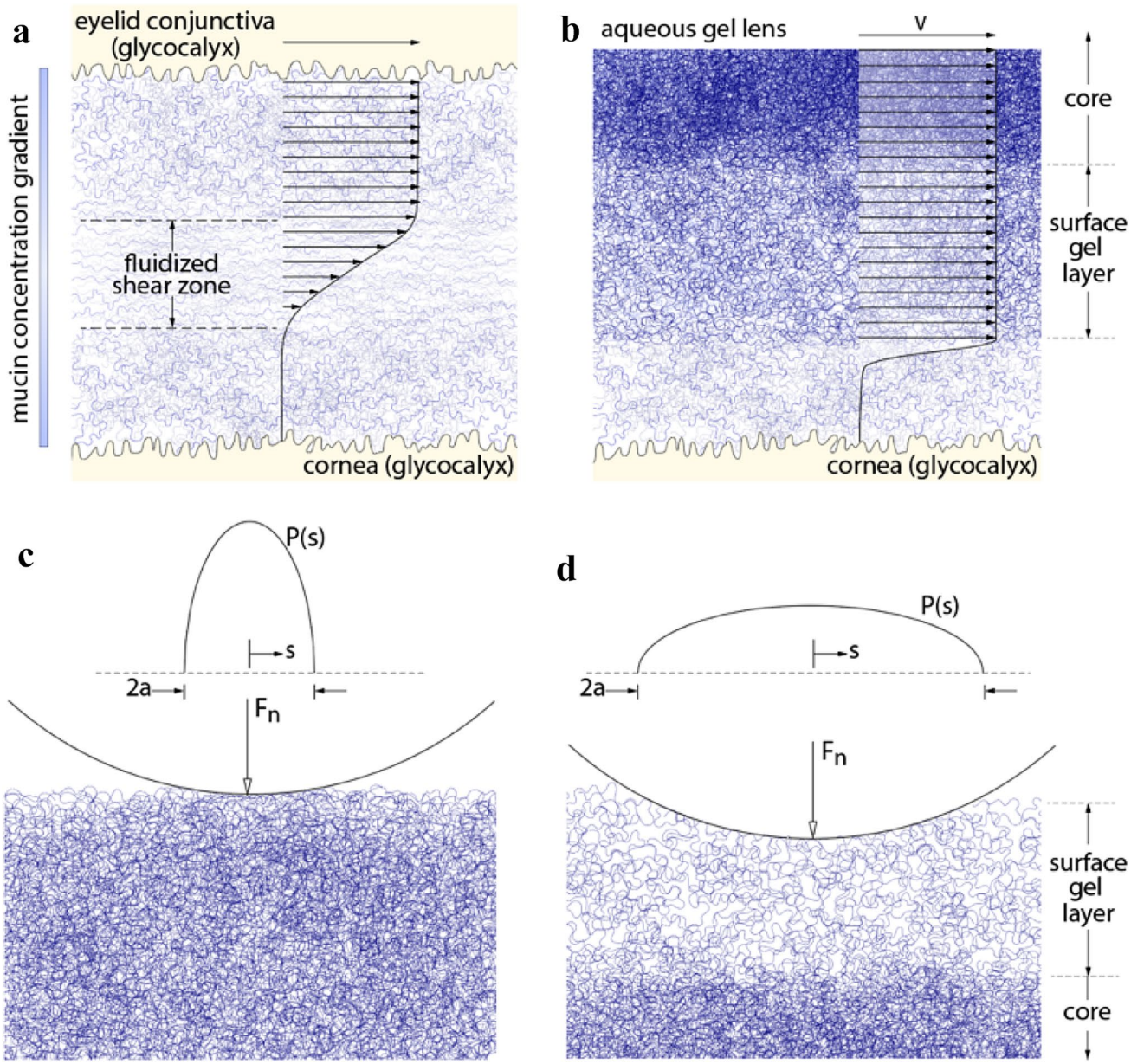

Fig. 1 **a** The natural tear film is a gel-spanning network with gradients in both mucin concentration and composition. This design undoubtedly produces gradients in yield stress, which may provide nearly constant shear stress over a range of sliding speeds. **b** Aqueous gel layers on the surfaces increase the water content and mesh size at the lens/cell interface as compared to silicone hydrogel (SiHy) core materials. **c** Schematic of a spherical contact against a SiHy material with a semi-elliptic contact pressure profile, *P(s)*, and finite contact width, 2*a*. **d** Schematic of contact against a surface gel layer, showing increased contact width, reduced contact pressure, and increased penetration into the gel layer

shear stress ($\tau \propto \xi^{-3}$) by increasing the contact area, decreasing the contact pressure, and dropping the friction coefficient [2]. This manuscript examines the sensitivity of corneal epithelial cell monolayers to direct contact sliding against five commercially available lens materials under physiologically relevant contact conditions (contact pressure, sliding speed, and duration). The materials were selected from three different manufacturers of daily disposable lenses and included both homogeneous material designs (three lenses, Fig. 1c) and surface gel layers (two lenses, Fig. 1d).

2 Methods

The cell model used in these experiments is based on a popular human telomerase-immortalized epithelial (hTCEpi) cell line, which has been extensively used to model corneal epithelial cell growth, proliferation, differentiation, desquamation, and mucin production [35]. Here a confluent cell monolayer was established following procedures and methods described previously on fibronectin-coated (EMD Millipore Corp FC010, at 0.2 mg/mL) glass-bottom culture dishes (20 mm in diameter); at confluence these culture dishes are covered by almost 1 million cells [5, 25, 36]. The cells were allowed to mature for 48 h to allow the mucin layer to develop and mature on the apical surfaces. During biotribological testing, the cells are maintained in a custom incubator over the microscope, which maintains the temperature (37 °C ± 0.1 °C), relative humidity (RH > 95%), and background pressure of CO_2 in otherwise ambient air (5% CO_2) [37]. The growth media is Keratinocyte Cell Basal Medium (KGB-Gold Cat#00192151) with 1% Penicillin–Streptomycin and 0.06 mM $CaCl_2$. The cells were limited to passage numbers 42–45, and each of the glass bottom culture plates were coated with a 200 µg/mL solution of fibronectin for 30 min, then rinsed with ultrapure water. Fibronectin, like collagen, is an extracellular matrix (ECM) protein that is a high molecular weight glycoprotein that binds to integrins. In our experience, this has been a reliable method of coating glass and preparing surfaces for corneal epithelial cell culture in monolayer, which is consistent with other groups' experiences [38, 39].

Biotribological testing was performed on the hTCEpi cell monolayers using an in situ biotribometer described in a number of publications [5, 25, 36, 37]. This instrument utilizes an ultra-low force dual-flexure cantilever to measure both the tangential and normal forces synchronously and dynamically. Contact lens specimens were cut from the central apex of lenses and mounted with the anterior surface exposed onto a spherically capped membrane probe assembly [40] made from pHEMA (65 wt% (hydroxyethyl)methacrylate (HEMA) crosslinked with 0.3 wt% *N,N′*-methylenebisacrylamide (MBAm)). The entire specimen assembly (Fig. 2) was equilibrated in PBS and soaked in bath of cell-growth media before mounting to the tribometer for testing and experiments. Depending on the particular experiment, the membrane probe thickness, *t*, was varied to control for contact pressure and permit lenses of different elastic modulus to be tested at the same force and contact pressure.

The contact lenses were aligned with their apex along the imaging axis of an inverted epifluorescent wide-field microscope. Contact area, cell motion, and probe movement could all be monitored in situ during testing. The hTCEpi monolayers were slid in reciprocating linear motion (3 mm stroke length) at a sliding speed of 1 mm/s for 1000 complete cycles. The average normal force was prescribed and controlled on a cycle-by-cycle basis for each experiment, and the contact pressure could be independently controlled and targeted by fabricating spherically capped membrane probes for each lens type to adjust for difference in elastic modulus and stiffness [40]. Friction forces were continuously measured synchronously with normal forces, and cyclic friction loops were confirmed for each cycle, and the friction coefficient was calculated for each cycle and recorded for the duration

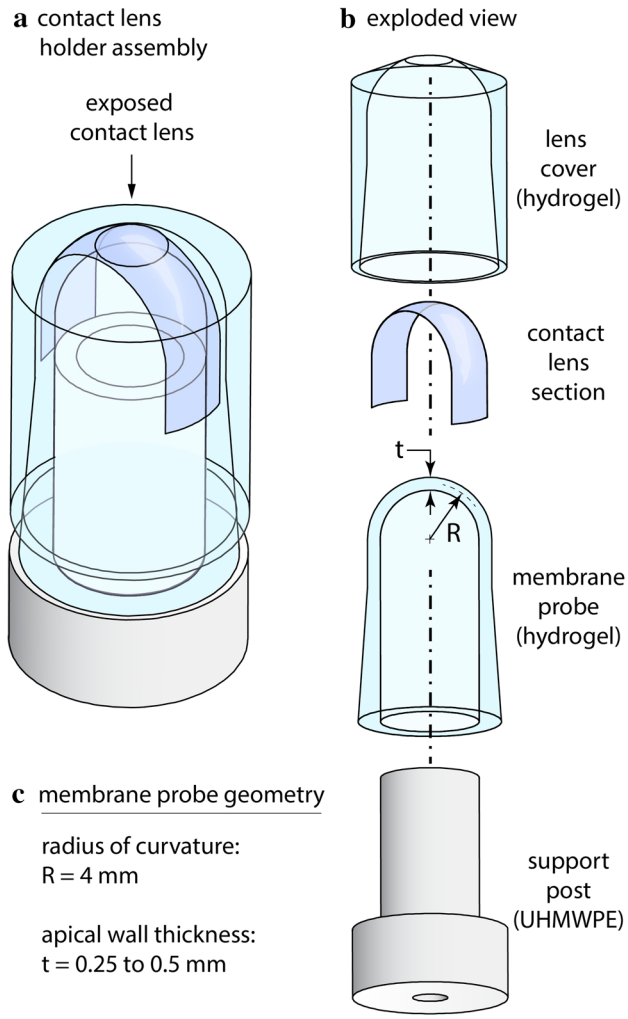

Fig. 2 Contact lens holder **a** assembly and **b** exploded view showing an exposed circular area of a contact lens section secured between a hydrogel lens cover and a spherical shell membrane hydrogel probe. The contact lens cover (holder) and membrane probe backing are composed of pHEMA. The assembly is mounted to an ultra-high molecular weight polyethylene (UHMWPE) support post which is fastened to the cantilever during testing. Typical membrane probe geometries listed in **c**

of the experiment. Associated uncertainties in the force measurements are propagated to give uncertainty intervals in both contact pressure and friction coefficient [41].

Periodically during testing, the entire contacting zone of the cell layer was imaged using the widefield inverted epifluorescent microscope. The composite image was created by "stitching" sequential image frames with 20% overlap across the entire field. The media was supplemented with two drops of propidium iodide, PI, (ReadyProbes Cell Viability Imaging Kit R37610), which was shown to be an outstanding indicator of cell damage under continuous exposure at low background level concentrations. This protocol was validated as a part of previous studies on friction-induced apoptosis using a suite of complementary techniques, including phosphatidylserine translocation, activated caspase 3/7 activity, imaging of actin depolymerization, and progression to secondary necrosis [36]. The image shown in Fig. 3a is a representative fluorescence microscopy image that overlays PI fluorescence (red: TRITC) with a brightfield image of the cells; PI is an intercalating agent that stains the nucleus of damaged cells. For the cells that stain positive for PI, both the periphery of the damaged cell and nuclear periphery are traced, as shown in Fig. 3b. The representative region analyzed in Fig. 3a, b, is indicated in a single widefield image Fig. 3c. After "stitching" together a number of images across the contact zone, the traced cells indicating PI damage are displayed without the brightfield images, Fig. 3d. These images are subsequently quantitatively analyzed to give numbers of cell damage as a function of sliding duration, materials, contact pressure, and shear stress.

To process larger amounts of imaging data, we developed an automated artificial intelligence package. As shown by the images in Fig. 3, the features of interest are typically small and localized. The feature detection and characterization algorithm (originally developed for astronomy research applications) identifies each individual feature, records the location, brightness, and basic shape characteristics. The algorithm applies a shallow neural network to classify each identified feature as either point-like or extended, with a probability associated to the classification. A separate machine-learning algorithm is then applied to the brightfield image, to trace the periphery of each cell providing a unique identifier and position/shape information for each cell in the image (typically ≈ 20,000 independent cells). This complementary computational analysis approach allows cross matching of the damaged cells (PI positive staining) and tracing of the cell nucleus and perimeter.

3 Results and Discussion

Representative composite images outlining cells that stain positive for PI (as described in the "Methods" section) after 1000 cycles of sliding at 200 μN are shown in descending order of damage in Fig. 4a. The astute observer may also discern a difference in cell size between the different

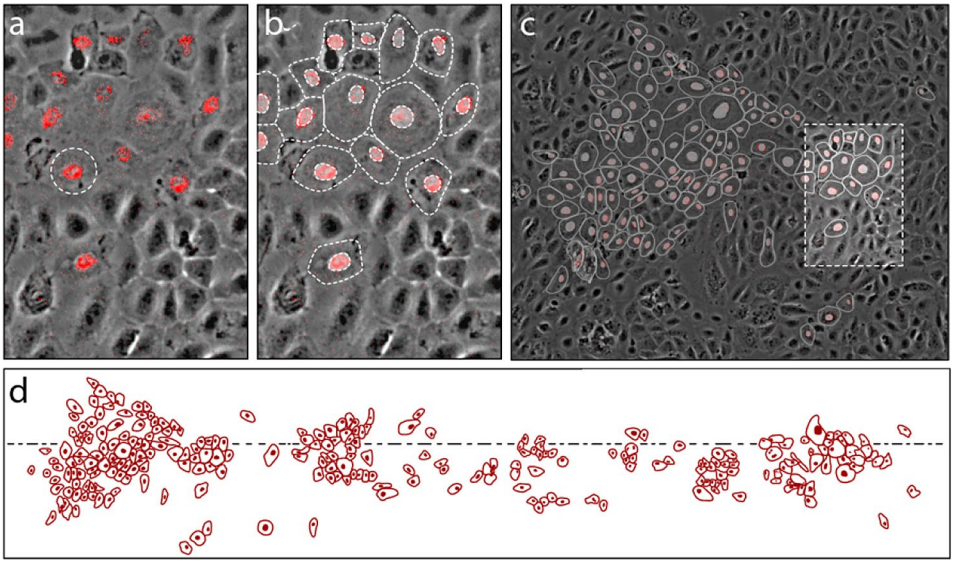

Fig. 3 **a** At discrete time points, hTCEpi cells are stained with propidium iodide (PI), which is a nuclear stain assay (red fluorescence) indicating cell damage. The white dashed circle indicates a cell with a compromised nucleus. **b** Cell nuclei and perimeters are traced by hand for damaged, PI-stained cells. **c** A larger image of the cells showing the inset of (**b**) within the measured field of cells—*approximately 400 cells within the image.* **d** A single composite image showing only the outlines of the cells that are positive for PI staining over the entire sliding track (stenfilcon A: 1000 cycles of sliding: normal force 200 μN, speed 1 mm/s, track length 3 mm, $\mu \approx 0.07$, and average contact pressure ≈ 1200 Pa) (Color figure online)

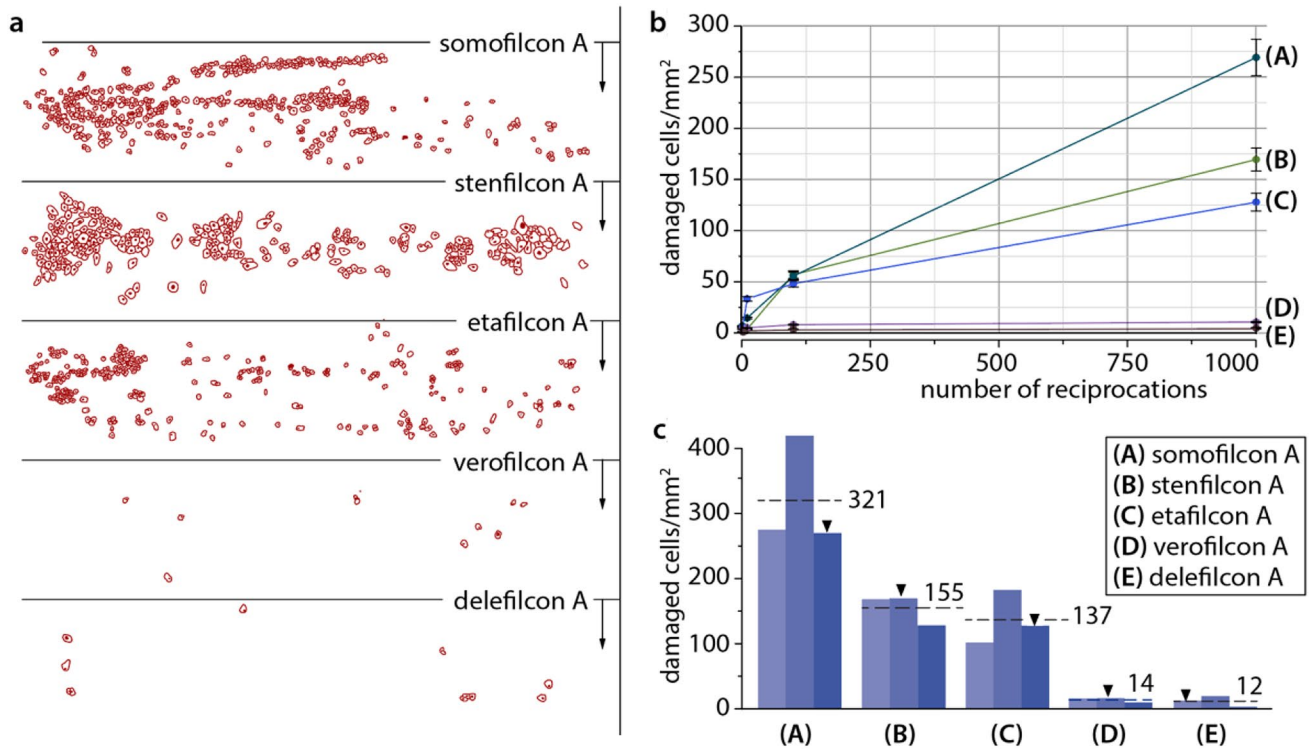

Fig. 4 **a** Composite image outlines of cell damage after 1000 sliding cycles for five different commercially available lens materials. **b** Analysis of the number of damaged cells per square millimeter of contact area, plotted for versus the number of sliding cycles. **c** Analysis of the number of damaged cells per square millimeter after 1000 sliding cycles (experiments performed in triplicate). Black arrowheads indicate the experiment that corresponds to the composite image illustrated to the left, the dashed line is the average value over three experiments. The baseline measurement of cell damage for experiments without sliding was 7 ± 4 cells per square millimeter

experiments, with the trend that the cells for the lenses with the most damage appear smaller than the others; this is actually due to a change in cell size during apoptosis, where during the programmed cell death process the cells contract and bleb—the cells are at different stages of apoptosis at the end of the sliding experiments. The average values of the normal force (F_n), friction coefficient (μ), average contact pressure ($<P>$), shear stress (τ), and density of damaged cells (#/mm^2) for these experiments are given in Table 1. The experiments were run in triplicate, and the associated experimental uncertainties, or standard deviation (whichever was larger), are also given in Table 1. Cell damage analysis and quantification (damaged cells/mm^2) was performed at 0, 10, 100, and 1,000 cycles of reciprocated sliding and these data are plotted in Fig. 4b along with the associated uncertainty intervals. The contact area in square millimeters was directly measured using a zero-order fringe contrast under the microscope. These data reveal a systematic increase in damage versus number of reciprocations, suggestive of damage associated with chronic stress [42]. The number of damaged cells per square millimeter are plotted for each experiment in bar graphs for lens materials A–E in Fig. 4c (each individual bar corresponds to a single experiment, and all three

Table 1 (Top) Results from experiments under controlled applied normal force, with contact pressure allowed to adjust depending on the mechanics of the individual lenses

	F_n (μN)	μ	$<P>$ (Pa)	τ (Pa)	#/mm^2
	Force-controlled experiments				
somofilcon A	200 ± 20	0.05	1,280 ± 60	64 ± 9	321 ± 69
stenfilcon A	200 ± 20	0.07	1,230 ± 80	86 ± 12	155 ± 19
etafilcon A	200 ± 20	0.08	595 ± 60	48 ± 7	137 ± 13
verofilcon A	200 ± 20	0.04	700 ± 40	28 ± 4	14 ± 4
delefilcon A	200 ± 20	0.04	400 ± 40	16 ± 2	12 ± 7
	Force- and contact pressure-controlled experiments				
etafilcon A	200 ± 20	0.07	400 ± 40	28 ± 4	126 ± 29
stenfilcon A	200 ± 20	0.07	400 ± 40	28 ± 4	58 ± 4
somofilcon A	200 ± 20	0.05	400 ± 40	20 ± 3	38 ± 10
delefilcon A	200 ± 20	0.04	400 ± 40	16 ± 2	12 ± 7
verofilcon A	200 ± 20	0.04	400 ± 40	16 ± 2	11 ± 4

(Bottom) Results from experiments under controlled applied normal force and contact pressure through the use of carefully designed membrane probes to match contact pressures across different lens materials. The materials are presented in order of descending severity for each experiment

experiments are shown as grouped by lens material. The average value of the measurand is indicated by the dashed horizontal line and given to the right by the accompanying value. The black arrowhead elements above individual bars indicate the experiment shown in Fig. 4a. There is a stark difference between the lenses with and without the surface gel layers; it was difficult to distinguish the damage associated with those lenses with the surface gel layers (verofilcon A and delefilcon A) from background apoptosis even after 1000 reciprocations. The background apoptosis (natural cell turnover) after 1 h 40 min (the duration of the 1000 cycle experiments) was measured to be 7 ± 4 cells/mm^2.

In prior work investigating friction-induced apoptosis with solid hydrogel probes, the cells were found to be sensitive to shear stress, and insensitive to direct contact pressure in the absence of sliding [36]. The average shear stress across the cell interface is a product of the average contact pressure and the friction coefficient. The friction coefficient is largely controlled by the polymer concentration in the lens materials (increasing mesh size, ξ, and water content reduces friction coefficient). The average contact pressure resulting from the same applied load is a very strong function of the elastic modulus of the materials, and as such is inversely proportional to the square of the mesh size, $\langle P \rangle \propto 1/\xi^2$; the result is that the lens materials that have a larger mesh-size and higher water content have both lower friction and a lower contact pressure [43, 44]. In an effort to evaluate the lens materials under equivalent contact pressures, individual membrane probes were made for each lens to independently set the contact pressures to 400 Pa at 200 µN of load. These experiments are therefore both force- and pressure-controlled, and the results are shown in Table 1. Experiments were again run in triplicate, following the same protocol and evaluated using the approach as presented in Fig. 3 and plotted in Fig. 4.

A one-way Analysis of Variance (ANOVA) test indicates an overall significance in variance between groups of $P < 0.0001$, indicating that the differences between the lens are statistically significant. Additionally, the Brown–Forsythe test reveals that there are no significant differences in standard deviations between groups, suggesting that the controlled experimental uncertainties are propagated evenly across the experimental set. Dunnet's corrected post-test analysis for significance comparing lenses without surface gel layers (stenfilcon A, somofilcon A, and etafilcon A) to lenses with surface gel layers (delefilcon A and verofilcon A) clearly indicated that there is a significant difference in cell damage between these two groups (adjusted P value < 0.001) with lenses having surface gel layers being more gentle and producing less damage on cell monolayers under shear than the traditional lenses without surface gel layers.

The results from the experiments controlling both the applied load and contact pressure are plotted in the bar graph in Fig. 5a. In contrast to the earlier experiments controlling only load, dropping the pressure for somofilcon A and stenfilcon A provided a significant reduction in cell damage. This impact of dropping contact pressures to 400 Pa for all of the materials is clearly evident in Fig. 5a, where the experiments under controlled force and contact pressure are shown in shades of gray next to the data plotted in Fig. 4c. It is also clear that materials with the highest friction coefficients were correlated with higher levels of cell damage. Over the past few years, shear stress has emerged as the driving factor in cell damage, whether in the production of genes associated with injury-induced remodeling [45], inflammation [25] apoptosis, or necrosis [36]. Calculations of the average shear stress, τ, for each experiment is provided in Table 1. Cell damage is plotted versus the average shear stress for all of the experiments in Fig. 5b. It is clear that cell damage increases with increasing shear stress. Although there is a guide line of slope = 3 on the log–log plot of cell

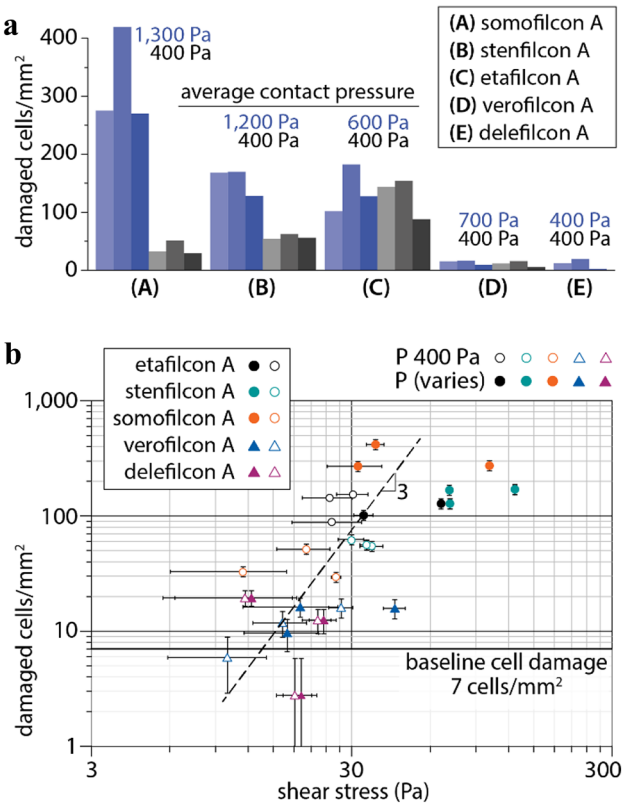

Fig. 5 **a** Bar graph of damaged cells per square millimeter for five commercially available lenses (A–C). All experiments were performed at 200 µN normal force in triplicate. (blue) Contact pressure depends on elastic modulus of the lens material. (gray) The membrane probe thickness was adjusted to give contact pressure of 400 Pa for the five different lens materials at the same 200 µN load. **b** Log–log plot of damaged cells per square millimeter for all lenses tested and all conditions versus average shear stress. Baseline cell damage without sliding is shown as the dark horizontal line at 7 cells/mm^2 (Color figure online)

damage versus shear stress we are not proposing a model for cell damage as a function of shear stress; rather, we propose that this is another indication that shear stress is the critical parameter from which to examine damage responses in the epithelial cells. It is also important to note that there is no correlation between friction coefficient and cell damage; for example, somofilcon A has an average friction coefficient of $\mu = 0.05$ across these experiments but the damage varies by over 8 × at the same normal force and the same friction coefficient—this is consistent with the trendline in Fig. 5 showing that the driver for this dramatic increase in damage is due to a 2 × increase in shear stress.

Examining the data in Table 1 is revealing, showing the strong dependence on contact pressure in the experiments that only control load, and the dependence on friction coefficient on the experiments controlling both load and contact pressure. The low levels of shear stress for verofilcon A and delefilcon A reveal the importance of trying to match the physiological levels of healthy tissue interfaces for biomedical devices. In contrast to load-bearing structural biological elements like bone, lubricating biological interfaces lack a robust "factor-of-safety" [46]. The healthy, physiologically "normal" levels of shear stress are the targeted values to minimize discomfort and cell damage—*biological evolution generally does not provide a wide range of capability or tolerance for elevated levels of shear stress*. Through this conceptual framework, the relationship between contact lens discomfort and dry eye discomfort emerges, and we suggest they may share a common etiology. Under conditions of shear stress above a tolerable limit, cells respond by releasing powerful signaling proteins responsible for discomfort, and if elevated levels of shear stress persist, cell damage accumulates with increasing concentrations of cytokines and DAMPs. The hypothesis is, therefore, that discomfort can be mitigated by lowering the shear stress in the ocular environment. Surface gel layers with a large polymer mesh size and high water content are one approach to lower the contact pressure, lower the friction coefficient, and thereby lower the shear stress [47].

4 Concluding Remarks

Cell monolayers of hTCEpi cells were used to examine the role of contact lens materials on cell damage under conditions of controlled contact pressure, sliding speed, and sliding duration. The results of these experiments showed increasing damage with increasing sliding duration and increasing shear stress. The lens materials that minimized cell damage had high water content surface gel layers, which are thought to reduce shear stress by reducing both the contact pressure and the friction coefficient. High water content surface gel layers have a large mesh size, resulting in a lower surface modulus and lower friction coefficient.

Acknowledgements The authors would like to thank Profs. Tommy E. Angelini and Brent Summerlin for sharing knowledge on mucins, biotribology, and gel physics. Additionally, the authors appreciate the many thoughtful discussions focused on contact lenses with Dr. Robert Tucker and Dr. John Pruitt from Alcon Vision, LLC. This research conducted in this manuscript was supported through a research grant from Alcon Vision, LLC.

References

1. Kogovšek, T., Tinta, T., Klun, K., Malej, A.: Jellyfish biochemical composition: importance of standardised sample processing. Mar. Ecol. Prog. Ser. **510**, 275–288 (2014). https://doi.org/10.3354/meps10959
2. Pitenis, A.A., Sawyer, W.G.: Lubricity of high water content aqueous gels. Tribol. Lett. **66**, 113 (2018). https://doi.org/10.1007/s11249-018-1063-5
3. Meldrum, O.W., Yakubov, G.E., Bonilla, M.R., Deshmukh, O., McGuckin, M.A., Gidley, M.J.: Mucin gel assembly is controlled by a collective action of non-mucin proteins, disulfide bridges, Ca2+-mediated links, and hydrogen bonding. Sci. Rep. **8**, 5802 (2018). https://doi.org/10.1038/s41598-018-24223-3
4. Argüeso, P., Gipson, I.K.: Epithelial mucins of the ocular surface: structure. Biosynthesis and function. Exp. Eye Res. **73**, 281–289 (2001). https://doi.org/10.1006/exer.2001.1045
5. Pitenis, A.A., Urueña, J.M., Hormel, T.T., Bhattacharjee, T., Niemi, S.R., Marshall, S.L., Hart, S.M., Schulze, K.D., Angelini, T.E., Sawyer, W.G.: Corneal cell friction: survival, lubricity, tear films, and mucin production over extended duration in vitro studies. Biotribology. **11**, 77–83 (2017). https://doi.org/10.1016/j.biotri.2017.04.003
6. Bron, A.J., Yokoi, N., Gaffney, E.A., Tiffany, J.M.: A solute gradient in the tear meniscus. I. A hypothesis to explain Marx's line. Ocul. Surf. **9**, 70–91 (2011). https://doi.org/10.1016/S1542-0124(11)70014-3
7. Bron, A.J., Yokoi, N., Gaffney, E.A., Tiffany, J.M.: A solute gradient in the tear meniscus. II. Implications for lid margin disease, including meibomian gland dysfunction. Ocul. Surf. **9**, 92–97 (2011). https://doi.org/10.1016/S1542-0124(11)70015-5
8. Willcox, M.D.P., Argüeso, P., Georgiev, G.A., Holopainen, J.M., Laurie, G.W., Millar, T.J., Papas, E.B., Rolland, J.P., Schmidt, T.A., Stahl, U., Suarez, T., Subbaraman, L.N., Uçakhan, O.Ö., Jones, L.: TFOS DEWS II tear film report. Ocul. Surf. **15**, 366–403 (2017). https://doi.org/10.1016/j.jtos.2017.03.006
9. Hodges, R.R.: Tear film mucins: front line defenders of the ocular surface; comparison with airway and gastrointestinal tract mucins. Exp. Eye Res. **117**, 62–78 (2013). https://doi.org/10.1016/j.exer.2013.07.027
10. King-Smith, P.E., Fink, B.A., Fogt, N., Nichols, K.K., Hill, R.M., Wilson, G.S.: The thickness of the human precorneal tear film: evidence from reflection spectra. Investig. Ophthalmol. Vis. Sci. **41**, 3348–3359 (2000)
11. Lai, S.K., Wang, Y.-Y., Wirtz, D., Hanes, J.: Micro- and macrorheology of mucus. Adv. Drug Deliv. Rev. **61**, 86–100 (2009). https://doi.org/10.1016/j.addr.2008.09.012
12. Gipson, I.K., Argüeso, P.: Role of mucins in the function of the corneal and conjunctival epithelia. International Review of Cytology Vol. 231, pp. 1–49. Academic Press, San Diego (2003)
13. Andrillon, T., Nir, Y., Cirelli, C., Tononi, G., Fried, I.: Single-neuron activity and eye movements during human REM sleep and awake

vision. Nat. Commun. **6**, 7884 (2015). https://doi.org/10.1038/ncomms8884
14. Dunn, A.C., Tichy, J.A., Sawyer, W.G., Urueña, J.M.: Lubrication regimes in contact lens wear during a blink. Tribol. Int. **63**, 45–50 (2013). https://doi.org/10.1016/j.triboint.2013.01.008
15. Pitenis, A.A., Urueña, J.M., Schulze, K.D., Nixon, R.M., Dunn, A.C., Krick, B.A., Sawyer, W.G., Angelini, T.E.: Polymer fluctuation lubrication in hydrogel gemini interfaces. Soft Matter **10**, 8955–8962 (2014). https://doi.org/10.1039/C4SM01728E
16. Kim, J., Dunn, A.C.: Thixotropic mechanics in soft hydrated sliding interfaces. Tribol. Lett. **66**, 102 (2018). https://doi.org/10.1007/s11249-018-1056-4
17. Giasson, S., Spencer, N.D.: Aqueous lubrication with polymer brushes. Aqueous Lubrication, p. 284. World Scientific Publishing Company, Singapore (2014)
18. Ma, L., Gaisinskaya-Kipnis, A., Kampf, N., Klein, J.: Origins of hydration lubrication. Nat. Commun. **6**, 1–6 (2015). https://doi.org/10.1038/ncomms7060
19. Gong, J.P., Iwasaki, Y., Osada, Y.: Friction of gels. 5. Negative load dependence of polysaccharide gels. J. Phys. Chem. B **104**, 3423–3428 (2000). https://doi.org/10.1021/jp992277v
20. Reale, E.R., Dunn, A.C.: Poroelasticity-driven lubrication in hydrogel interfaces. Soft Matter **13**, 428–435 (2017). https://doi.org/10.1039/C6SM02111E
21. Urueña, J.M., Pitenis, A.A., Nixon, R.M., Schulze, K.D., Angelini, T.E., Sawyer, W.G.: Mesh size control of polymer fluctuation lubrication in gemini hydrogels. Biotribology **1–2**, 24–29 (2015). https://doi.org/10.1016/j.biotri.2015.03.001
22. de Beer, S., Müser, M.H.: Alternative dissipation mechanisms and the effect of the solvent in friction between polymer brushes on rough surfaces. Soft Matter **9**, 7234 (2013). https://doi.org/10.1039/c3sm50491c
23. Moore, A.C., Burris, D.L.: An analytical model to predict interstitial lubrication of cartilage in migrating contact areas. J. Biomech. **47**, 148–153 (2014). https://doi.org/10.1016/j.jbiomech.2013.09.020
24. Jones, L., Brennan, N.A., González-Méijome, J., Lally, J., Maldonado-Codina, C., Schmidt, T.A., Subbaraman, L., Young, G., Nichols, J.J.: The TFOS international workshop on contact lens discomfort: report of the contact lens materials, design, and care subcommittee. Investig. Opthalmol. Vis. Sci. (2013). https://doi.org/10.1167/iovs.13-13215
25. Pitenis, A.A., Urueña, J.M., Hart, S.M., O'Bryan, C.S., Marshall, S.L., Levings, P.P., Angelini, T.E., Sawyer, W.G.: Friction-induced inflammation. Tribol. Lett. **66**, 81 (2018). https://doi.org/10.1007/s11249-018-1029-7
26. Cook, A.D., Christensen, A.D., Tewari, D., McMahon, S.B., Hamilton, J.A.: Immune cytokines and their receptors in inflammatory pain. Trends Immunol. **39**, 240–255 (2018). https://doi.org/10.1016/j.it.2017.12.003
27. Belmonte, C., Acosta, M.C., Merayo-Lloves, J., Gallar, J.: What causes eye pain? Curr. Ophthalmol. Rep. **3**, 111–121 (2015). https://doi.org/10.1007/s40135-015-0073-9
28. Belmonte, C., Aracil, A., Acosta, M.C., Luna, C., Gallar, J.: Nerves and sensations from the eye surface. Ocul. Surf. **2**, 248–253 (2004). https://doi.org/10.1016/S1542-0124(12)70112-X
29. Efron, N.: Contact lens wear is intrinsically inflammatory. Clin. Exp. Optom. **100**, 3–19 (2017). https://doi.org/10.1111/cxo.12487
30. Dunn, A.C., Urueña, J.M., Huo, Y., Perry, S.S., Angelini, T.E., Sawyer, W.G.: Lubricity of surface hydrogel layers. Tribol. Lett. **49**, 371–378 (2013). https://doi.org/10.1007/s11249-012-0076-8
31. Pitenis, A.A., Urueña, J.M., Cooper, A.C., Angelini, T.E., Sawyer, W.G.: Superlubricity in gemini hydrogels. J. Tribol. **138**, 042103 (2016). https://doi.org/10.1115/1.4032890
32. Schulze, K.D., Hart, S.M., Marshall, S.L., O'Bryan, C.S., Urueña, J.M., Pitenis, A.A., Sawyer, W.G., Angelini, T.E.: Polymer osmotic pressure in hydrogel contact mechanics. Biotribology **11**, 3–7 (2017). https://doi.org/10.1016/j.biotri.2017.03.004
33. Meier, Y.A., Zhang, K., Spencer, N.D., Simic, R.: Linking friction and surface properties of hydrogels molded against materials of different surface energies. Langmuir **35**, 15805–15812 (2019). https://doi.org/10.1021/acs.langmuir.9b01636
34. Gombert, Y., Simič, R., Roncoroni, F., Dübner, M., Geue, T., Spencer, N.D.: Structuring hydrogel surfaces for tribology. Adv. Mater. Interfaces **6**, 1901320 (2019). https://doi.org/10.1002/admi.201901320
35. Robertson, D.M., Li, L., Fisher, S., Pearce, V.P., Shay, J.W., Wright, W.E., Cavanagh, H.D., Jester, J.V.: Characterization of growth and differentiation in a telomerase-immortalized human corneal epithelial cell line. Investig. Opthalmol. Vis. Sci. **46**, 470 (2005). https://doi.org/10.1167/iovs.04-0528
36. Hart, S.M., Degen, G.D., Urueña, J.M., Levings, P.P., Sawyer, W.G., Pitenis, A.A.: Friction-induced apoptosis. Tribol. Lett. **67**, 82 (2019). https://doi.org/10.1007/s11249-019-1197-0
37. Urueña, J.M., Hart, S.M., Hood, D.L., McGhee, E.O., Niemi, S.R., Schulze, K.D., Levings, P.P., Sawyer, W.G., Pitenis, A.A.: Considerations for biotribometers: cells, gels, and tissues. Tribol. Lett. **66**, 141 (2018). https://doi.org/10.1007/s11249-018-1094-y
38. Yamamoto, A., Mishima, S., Maruyama, N., Sumita, M.: Quantitative evaluation of cell attachment to glass, polystyrene, and fibronectin- or collagen-coated polystyrene by measurement of cell adhesive shear force and cell detachment energy. J. Biomed. Mater. Res. **50**, 114–124 (2000). https://doi.org/10.1002/(SICI)1097-4636(200005)50:2<114:AID-JBM4>3.0.CO;2-6
39. Lacouture, M.E., Schaffer, J.L., Klickstein, L.B.: A comparison of type I collagen, fibronectin, and vitronectin in supporting adhesion of mechanically strained osteoblasts. J. Bone Miner. Res. **17**, 481–492 (2002). https://doi.org/10.1359/jbmr.2002.17.3.481
40. Marshall, S.L., Schulze, K.D., Hart, S.M., Urueña, J.M., McGhee, E.O., Bennett, A.I., Pitenis, A.A., O'Bryan, C.S., Angelini, T.E., Sawyer, W.G.: Spherically capped membrane probes for low contact pressure tribology. Biotribology **11**, 69–72 (2017). https://doi.org/10.1016/j.biotri.2017.03.008
41. Schmitz, T.L., Action, J.E., Ziegert, J.C., Sawyer, W.G.: The difficulty of measuring low friction: uncertainty analysis for friction coefficient measurements. J. Tribol. **127**, 673 (2005). https://doi.org/10.1115/1.1843853
42. Sterner, O., Aeschlimann, R., Zürcher, S., Scales, C., Riederer, D., Spencer, N.D., Tosatti, S.G.P.: tribological classification of contact lenses: from coefficient of friction to sliding work. Tribol. Lett. **63**, 9 (2016). https://doi.org/10.1007/s11249-016-0696-5
43. Gong, J.P.: Friction and lubrication of hydrogels—its richness and complexity. Soft Matter **2**, 544 (2006). https://doi.org/10.1039/b603209p
44. Shoaib, T., Heintz, J., Lopez-Berganza, J.A., Muro-Barrios, R., Egner, S.A., Espinosa-Marzal, R.M.: Stick-slip friction reveals hydrogel lubrication mechanisms. Langmuir **34**, 756–765 (2018). https://doi.org/10.1021/acs.langmuir.7b02834
45. Correro-Shahgaldian, M.R., Colombo, V., Spencer, N.D., Weber, F.E., Imfeld, T., Gallo, L.M.: Coupling plowing of cartilage explants with gene expression in models for synovial joints. J. Biomech. **44**, 2472–2476 (2011). https://doi.org/10.1016/j.jbiomech.2011.06.021
46. Diamond, J.: Quantitative evolutionary design. J. Physiol. **542**, 337–345 (2002). https://doi.org/10.1113/jphysiol.2002.018366
47. Chau, A.L., Rosas, J., Degen, G.D., Månsson, L.K., Chen, J., Valois, E., Pitenis, A.A.: Aqueous surface gels as low friction interfaces to mitigate implant-associated inflammation. J. Mater. Chem. B **8**, 6782–6791 (2020)

Publisher's Note Springer Nature remains neutral with regard to jurisdictional claims in published maps and institutional affiliations.